ADVANCED MATERIALS
www.advmat.de

Transparent, High-Performance Thin-Film Transistors with an InGaZnO/Aligned-SnO_2-Nanowire Composite and their Application in Photodetectors

Xingqiang Liu, Xi Liu, Jingli Wang, Chongnan Liao, Xiangheng Xiao, Shishang Guo, Changzhong Jiang, Zhiyong Fan, Ti Wang, Xiaoshuang Chen, Wei Lu, Weida Hu, and Lei Liao**

Thin-film transistors (TFTs) based on amorphous silicon and poly-silicon have become the key components of a myriad of electronics and photonics devices including displays and sensors, for a wide range of applications such as computers and cell phones.[1,2] With the continuous technological advancement, high-current-density TFTs are in urgent need for high-brightness flat-panel displays and high-speed radiofrequency identification.[3,4] However, amorphous-silicon-based TFTs present the limitations of a low carrier mobility (~1 cm^2 V^{-1} s^{-1}) accompanied by light degradation.[5,6] In spite of possessing high carrier mobility, the opacity of TFTs based on polycrystalline silicon (poly-silicon) restricts the aperture ratio for active matrix arrays, and the spatial distribution of the poly-silicon grain structure results in non-uniform device performance over large areas, which limits the scalable fabrication.[7] As one of the alternative materials, amorphous metal oxides have attracted increasing attention during the past few years, and they are being extensively researched today as the most promising candidates for the next generation of flat-panel displays. In fact, they not only outperform amorphous silicon in conventional applications, but they also open a door to completely new and groundbreaking areas such as paper electronics.[8,9] The alluring merits of these amorphous metal oxides are high optical transparency, desirable mobility, and an amorphous microstructure, e.g., amorphous InGaZnO (a-IGZO).[7,10] However, high-speed circuitry requires TFTs to operate at a high on-current, thus it is important to continue to significantly improve the performance of a-IGZO TFTs, especially with respect to mobility and saturation current.[11,12] On the other hand, although 1D crystalline nanowires (NWs) have been employed to fabricate high-performance TFTs,[13] it was found that the channel length needed to be shorter than the length of the NWs in order to achieve efficient utilization of the NWs, which leads to the challenge for scalable fabrication.[14–16] In our previous work,[11] single-wall carbon nanotubes (SWNTs) were incorporated into a-IGZO, which had substantially improved the mobility of the earlier a-IGZO thin film. However, due to the ratio between the metallic and semiconducting SWNTs being about 1:2, a metallic conducting network in the a-IGZO/SWNT composite thin film was formed. Therefore, the short-channel effect and electrostatic screening effect were observed for the a-IGZO/SWNT TFTs, weakening the gate electrostatic control. All of these characteristics have led to an evolution from semiconducting to metallic properties in the composite thin films as the channel length decreased. To avoid this undesirable behavior, herein, a combined sol–gel and contact-printing method was employed to incorporate high-mobility aligned SnO_2 NWs into a-IGZO thin films for fabricating high-mobility TFTs, so that the advantages of the a-IGZO film (i.e., large-scale fabrication) and NWs (i.e., high mobility) could be combined. The incorporated aligned SnO_2 NWs result in the successful fabrication of the a-IGZO/(aligned-SnO_2-NW) composite TFTs with an enhanced field-effect mobility of 109.0 cm^2 V^{-1} s^{-1} and a high current density of 61.4 μA $μm^{-1}$ for 10-μm channels. The performance surpassed that of single-crystalline InGaZnO TFTs with a mobility ~80 cm^2 V^{-1} s^{-1}, which typically has a high-temperature epitaxial layer.[17] Additionally, it is comparable to that of low-temperature poly-silicon with a mobility in the range of 50–100 cm^2 V^{-1} s^{-1} and a current density of 0.1–100 μA $μm^{-1}$.[18–20] Aside from being environmentally friend and of low cost, this new a-IGZO/(aligned-SnO_2-NW) composite system can also be used to fabricate a high-performance UV photodetector, which we will also demonstrate here.

Crystalline SnO_2 NWs were prepared on 1-nm Au-coated Si substrates using the typical chemical vapor deposition method.[21] The scanning electron microscopy (SEM) image and X-ray diffraction spectra are available in the Supporting Information (SI; Figure S1a,b). A single SnO_2 NW possesses a high mobility of 140.6 cm^2 V^{-1} s^{-1}; the typical transfer and output characteristics of a single-SnO_2-NW transistor can be found in the SI (Figure S1c,d). **Figure 1** illustrates the method for fabricating a-IGZO/(SnO_2-NW) composite TFTs. Briefly,

Dr. X. Q. Liu, Dr. J. L Wang, Dr. C. N. Liao, Prof. X. H. Xiao, Prof. S. S. Guo, Prof. C. Z. Jiang, Dr. T. Wang, Prof. L. Liao
Department of Physics and Key Laboratory of Artificial Micro- and Nano-structures of Ministry of Education
Wuhan University
Wuhan 430072, China
E-mail: liaolei@whu.edu.cn
Prof. X. S. Chen, Prof. W. Lu, Prof. W. D. Hu
National Laboratory for Infrared Physics
Shanghai Institute of Technical Physics
Chinese Academy of Sciences
Shanghai 200083, China
E-mail: wdhu@mail.sitp.ac.cn
X. Liu, Prof. Z. Y. Fan
Department of Electronic & Computer Engineering
The Hong Kong University of Science & Technology
Hong Kong SAR, China

DOI: 10.1002/adma.201401732

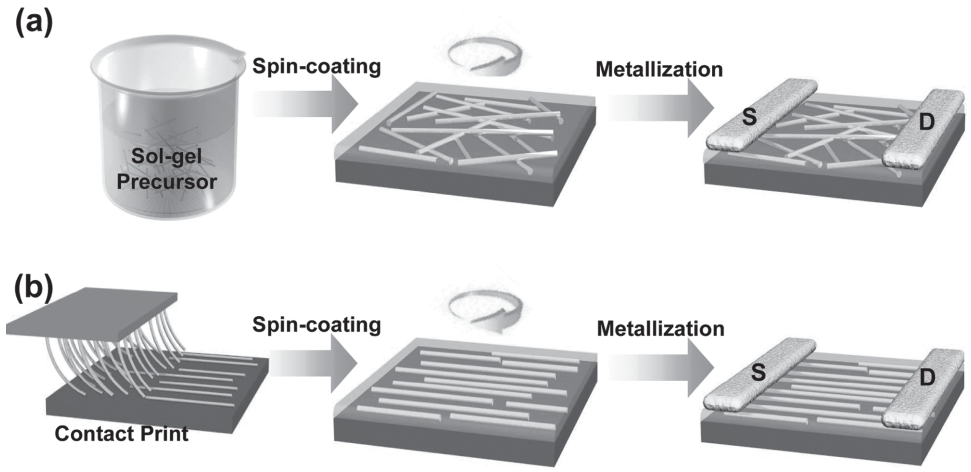

Figure 1. Schematic illustration of the fabrication process for obtaining the a-IGZO/(SnO_2-NW) composite thin film transistors (TFTs). a) The as-prepared SnO_2 NWs are introduced into a-IGZO precursor and ultrasonically dispersed, so as to achieve a uniform composite precursor. Then a-IGZO/(random-SnO_2-NW) composite thin films are obtained through a spin-coating approach. Finally, the TFTs structure is completed by metallization. b) The contact-printing method is conducted to align the SnO_2 NWs, and then the a-IGZO thin film is spin-coated. Finally, the a-IGZO/(aligned-SnO_2-NW) TFT structure is completed by metallization.

the a-IGZO precursor was prepared by adding indium nitrate, gallium nitrate, and zinc acetate at a fixed molar ratio of 1:1:1. Subsequently, the as-prepared NWs were dispersed into the precursor with specified weight concentrations so that the incorporated NWs were randomly dispersed into the a-IGZO. For fabricating the a-IGZO/(aligned-SnO_2-NW) composite TFTs, a contact-printing method was conducted to arrange the SnO_2 NWs in good alignment.[22–24] Finally, the Cr/Au electrodes for source (S) and drain (D) electrodes were completed by the typical photolithography, metallization, and lift-off process

Figure 2a–c present the SEM images of the a-IGZO/(random-SnO_2-NW) composite thin films with different SnO_2 NW densities. By controlling the contact-printing pressure, we also achieved similar densities for composites with the aligned NWs, as shown in Figure 2d–f. Electrical measurements were carried out under dark conditions to evaluate the effects of the incorporated crystalline SnO_2 NWs in a-IGZO/(SnO_2-NW) composite thin films.

Typical transfer curves of the a-IGZO/(random-SnO_2-NW) TFTs with different SnO_2 NW densities are shown in **Figure 3**a. It is clearly shown that the on-current is significantly enhanced by incorporation of the SnO_2 NWs. Figure 3b summarizes the influence of incorporated SnO_2 NWs in a-IGZO thin films. The composite TFTs demonstrate elevated mobility with an increase of SnO_2-NW density in the range of 0–15 NWs μm^{-1} and reach a value of 62.4 $cm^2\ V^{-1}\ s^{-1}$, after which it decreases as the

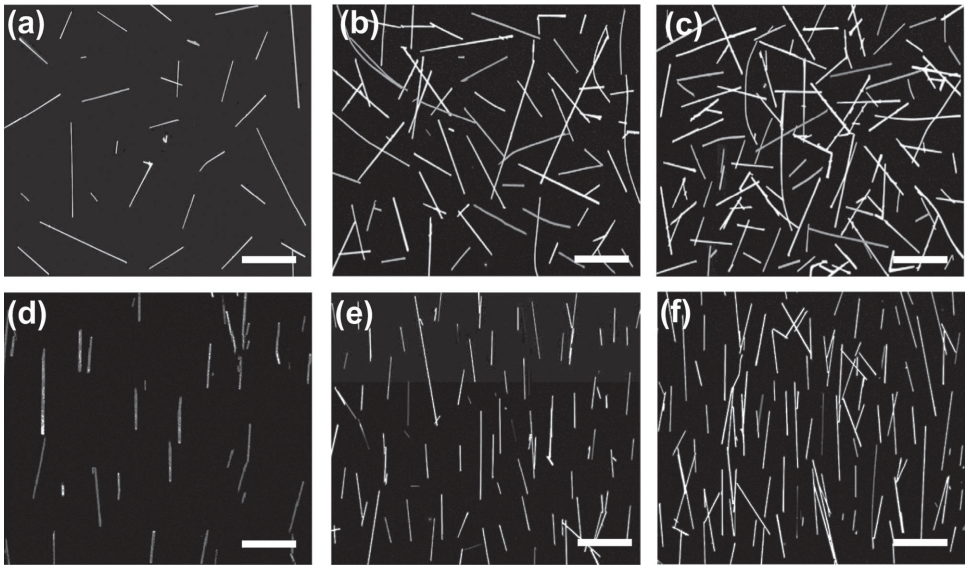

Figure 2. SEM images of a-IGZO/(SnO_2-NW) composite thin films with different NW densities; scale bars are 10 μm. a–c) Films with SnO_2 NWs randomly dispersed into the composite thin films; the NW density is ~4 (a), ~10 (b), and ~15 (c) NWs μm^{-1}. d–f) Films with aligned SnO_2 NWs in the composite thin films; the NW density is ~5 (d), ~11 (e), and ~16 (f) NWs μm^{-1}.

Adv. Mater. **2014**,
DOI: 10.1002/adma.201401732

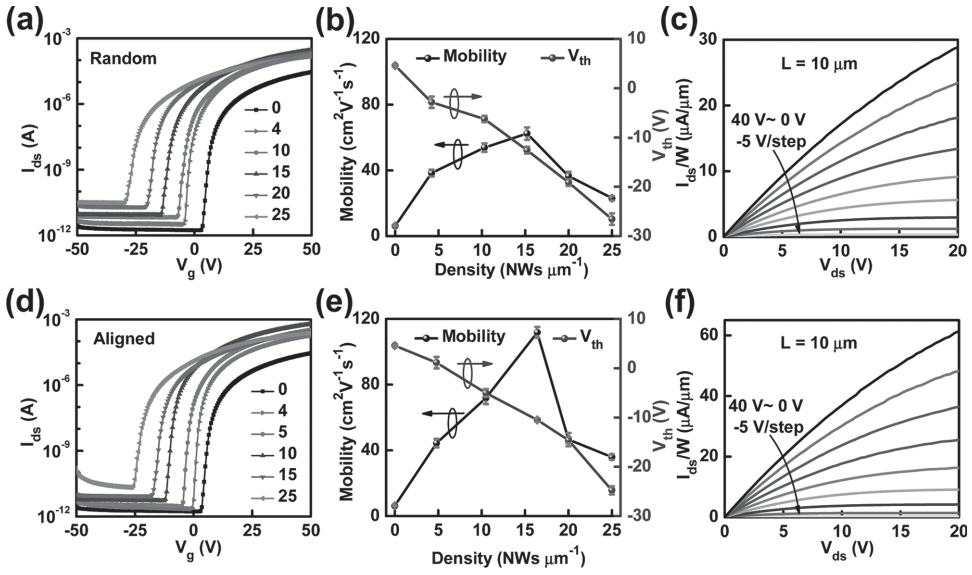

Figure 3. Typical electrical characteristics of a-IGZO/(SnO_2-NW) composite TFTs with different SnO_2 NW densities. a) Transfer characteristics (with the on-current density (I_{ds}/W) plotted logarithmically at V_{ds} = 1 V; I_{ds} and W represent the drain–source on-current and the channel width, respectively) of the a-IGZO/(random-SnO_2-NW) composite TFTs. V_g represents the gate voltage; the legend numbers indicate the NW density per micrometer. b) Plots of the mobility and V_{th} versus SnO_2 NW density. c) Typical output characteristics of the a-IGZO/(random-SnO_2-NW) composite TFTs with ~15 NWs μm^{-1}. d) Transfer characteristics of the a-IGZO/(aligned-SnO_2-NW) composite TFTs obtained at V_{ds} = 1 V. The legend numbers indicate the NW density per micrometer. e) Plots of the mobility and V_{th} versus aligned NW density. f) Typical output characteristics of the a-IGZO/(aligned-SnO_2-NW) composite TFTs with ~16 NWs μm^{-1}.

SnO_2-NW density continues to increase, while the threshold voltage (V_{th}) drifts to much more negative values as the SnO_2-NW density increases. Figure 3c shows the output characteristics of the maximum mobility TFTs with 15 NWs um^{-1} for the NW density. It is indicated that the composite channel can be clearly pinched off by the gate potential. A similar effect has been observed for the a-IGZO/(aligned-SnO_2-NW) composite TFTs. Moreover, as shown in Figure 3d and e, the mobility of the a-IGZO/(aligned-SnO_2-NW) composite TFTs is further enhanced compared to the a-IGZO/(random-SnO_2-NW) composite TFTs, with a maximum value of 109.0 cm^2 V^{-1} s^{-1}. The V_{th} of the device with maximum mobility is smaller than that of the a-IGZO/(aligned-SnO_2-NW) composite TFTs with the same NW density. Figure 3f presents a high current density of 61.4 μA μm^{-1} with 10-μm channels for an a-IGZO/(aligned-SnO_2-NW) composite TFT at drain–source voltage of V_{ds} = 20 V. This value is higher than those that have been previously reported for amorphous-oxide-based TFTs, which typically exhibited a current density of less than 5 μA μm^{-1}.[7,25,26] Overall, the SnO_2 NWs enhanced the performance compared to pristine a-IGZO TFTs. And by aligning the NWs in the composite channel, performance can be further boosted. This phenomenon can be understood as following: in the composite TFTs with randomly dispersed NWs, at the on-state, the crystalline oxide NWs shorten the channel length and provide the fast carrier transport tracks at low concentration.[27] Additionally, the a-IGZO parts connect these fast carrier transport tracks, further enhancing the current in the conductive channel (SI: Figure S2a). Moreover, with the aligned NWs in the composite channel, the efficient carrier transport tracks are further shortened, leading to much higher mobility (SI: Figure S2b). Meanwhile, the good alignment of the NWs avoids cross stacking of NWs on top of each other, which can further help to improve gate electrostatic coupling.[22] In the other words, the a-IGZO and SnO_2 NWs are complementary to each other in the composite thin films. At low NW density, these SnO_2 NWs provided a positive contribution to TFT performance. The SnO_2 NWs provide the fast carrier transportation paths and the a-IGZO fills the space between the NWs and connects them to form a continuous composite thin film, leading to the enhanced current density (Figure S2c). Once the SnO_2-NW loading reaches a critical density, the enhancement effect is maximized. For SnO_2-NW loading beyond that critical threshold, the portion of the a-IGZO is progressively reduced, because more and more free space is occupied by the high-density SnO_2 NWs.[28] The active channel becomes a random combination of numerous smaller parts of a-IGZO and SnO_2 NWs (SI: Figure S2d). This might result in large interfacial roughness, leading to increased carrier traps and scattering. Therefore, the contact resistance between a-IGZO and SnO_2 NWs is increased and the injection of carriers is inhibited, leading to the inferior TFT performance.[29] As a result, incorporating low-density SnO_2 NWs could lead to improved TFT performance (Figure S3a,b), while the high-density SnO_2 NWs could degrade the TFT mobility. Meanwhile, the defects in the composite system could lead to the drift of the V_{th} towards the negative axis as concentration increases.[12] Generally, by aligning the NWs in the composite channel, the efficient carrier transport tracks are further shortened and the number of defects is decreased correspondingly. Thus the composite TFTs with aligned NWs demonstrate more preferable performance as compared to both the pristine a-IGZO and the a-IGZO/(random-SnO_2-NW) composite TFTs.

We experimentally investigated the heterojunction between a single SnO_2 NW and the a-IGZO film, and **Figure 4**a is the

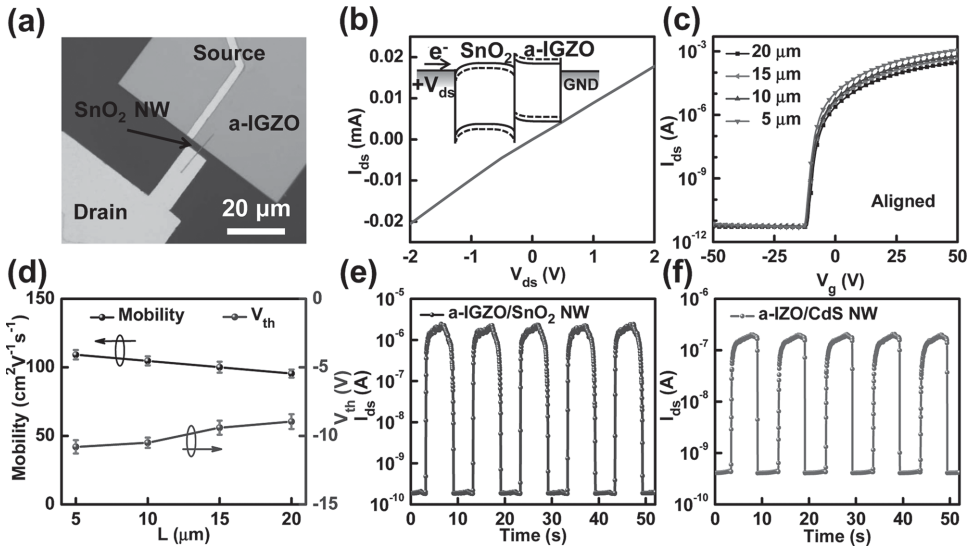

Figure 4. a) Optical image of the device comprising a single SnO_2 NW and the a-IGZO film. b) *I–V* curve of the fabricated device, and the linear characteristics indicate that Ohmic contacts were formed at all metal/semiconductor interfaces. Inset: band alignment of the composite system (GND is the abbreviation of ground). c) Typical transfer characteristics of the aligned a-IGZO/(SnO_2-NW) composite TFTs with different channel lengths; the NW density was fixed to ~16 NWs μm^{-1} in the composite channels. d) Plot of the mobility and V_{th} versus channel length. e) The on–off photoresponse of the a-IGZO/(aligned-SnO_2-NW) composite TFTs with a NW density of ~16 NWs μm^{-1} in the composite channels. The incident light wavelength was 350 nm with of power intensity of P_{light} = 1 mW cm^{-2}, W = 70 μm, and L = 10 μm; the V_g = −12 V and V_{ds} = 0.1 V were set to read out the signal. f) The time-dependent *I–V* characteristics of the optimized a-IZO/(aligned-CdS-NW) composite TFTs.

optical image of the fabricated device. In the device, the difference in work functions may lead to potential barriers formed at the SnO_2/a-IGZO interface (inset in Figure 4b).[30,31] However, due to the relatively small work-function mismatch, although photo-carriers may accumulate at the a-IGZO/NW interface, the *I–V* measurements in Figure 4b indicate that electrons can still be effectively injected into SnO_2 in the on-state, so the photogating effect, which was observed in a hybrid system,[32] could be neglected. On the other hand, when a positive voltage was applied to the a-IGZO thin film, the height of potential barriers increased (dashed line in the inset of Figure 4b), leading to the forward current being slightly smaller than the reverse current. No obvious rectification characteristics were observed in the *I–V* measurements of the fabricated device, and nearly ohmic contacts were formed in all parts of the device.[33,34] Thus the carriers can be highly efficiently injected and transported through the a-IGZO/(SnO_2-NW) composite layer, enabling a high current density and mobility. To probe the reliability and channel length scaling of the a-IGZO/(SnO_2-NW) composite TFTs, we fabricated and studied a-IGZO/(aligned-SnO_2-NW) composite TFTs with a channel length (L) varying from 5 to 20 μm. Figure 4c compares the transfer characteristics. Figure 4d summarizes the mobility and V_{th} versus L. The field-effect mobility of the TFTs was observed to slightly increase as the channel length shrinks. As the channel length decreases, more and more NWs percolate the composite channel, and then the SnO_2 NWs dominate the composite channel, leading to the much higher mobility of the a-IGZO/(aligned-SnO_2-NW) composite TFTs, approaching that of aligned-NW TFTs (Figure S3c,d). To some degree, the percolated NWs are more effective than the unpercolated NWs on the mobility of the TFTs (see SI: Table S1 and S2). As aforementioned, the a-IGZO/SWNT composite TFTs become more metallic as the channel length is decreased.[11] On the other hand, the current-enhanced paths were supplied by the semiconducting SnO_2 NWs in the a-IGZO/(aligned-SnO_2-NW) TFTs. Therefore, the a-IGZO/(aligned-SnO_2-NW) TFTs have eliminated the percolation effect and electrostatic screening effect, resulting in superior scaling performance, which is also observed for the a-IGZO/(random-SnO_2-NW) TFTs (SI: Figure S4a,b).

a-IGZO has also shown great potential in applications for optoelectronic components. It has been widely explored for phototransistors due to their high sensitivity to UV light and excellent electrical characteristics (such as high on–off ratio) for integrated circuits.[35–37] However, the photocurrent (I_{ph}) is determined by $I_{ph} = \mu_{eff} \Delta Q_n V_{ds} W/L$,[38] where μ_{eff} is the effective mobility, Q_n is the magnitude of the areal charge density of a-IGZO, and W and L are the channel width and length, respectively. This indicates that I_{ph} is proportional to μ_{eff} under the same illumination conditions at fixed bias voltages. Therefore, low mobility results as a result of the low photosensitivity of a-IGZO TFTs to UV light.[39] The extracted responsivity of the pristine a-IGZO is only 8.3 A W^{-1} (SI: Figure S5a). On the other hand, with the combination of long lifetime and short transit time of the charge carriers, 1D crystalline NWs photodetector have substantial photoconductive gain.[40–42] Measurements of the time-dependent photocurrent was conducted for the a-IGZO/(aligned-SnO_2-NW) composite TFTs. By using the conventional model for the responsivity (R_{ph}) calculation [$R_{ph} = I_{ph}/(P_{light}LW) = (|I_{light} - I_{dark}|)/(P_{light}LW)$], where I_{ph} is the photocurrent, I_{light} is the drain current under illumination, I_{dark} the drain current in the dark, P_{light} is the light power intensity, L is the channel length of the device, and W is the channel width of the device. When the a-IGZO/(SnO_2-NW) composite TFTs were illuminated by a 350-nm-wavelength laser source, a specific V_g of −12 V was required to deplete the channel

Adv. Mater. 2014,
DOI: 10.1002/adma.201401732

carriers to maximize the photocurrent gain,[43,44] allowing the photogenerated carriers to drift through the channel. In this scheme, the photoresponse ratio (I_{ph}/I_{dark}) is much more sensitive to the carrier-concentration change caused by light illumination. Finally, the signal can be read by applying V_{ds} = 0.1 V voltage. The calculated photoresponsivity value at the wavelength of 350 nm is ~328.6 A W^{-1}, which is extracted from the time-dependent *I–V* curve in Figure 4e. This value is larger than that of conventional UV photodetectors (typically <10 A W^{-1}).[45–47] On the other hand, in our previous work,[44] a 5.8 A W^{-1} responsivity and a high mobility of 27.1 cm^2 V^{-1} s^{-1} were obtained under 445-nm light illumination in TFTs based on a composite of amorphous InZnO and CdS NWs (a-IZO/CdS NW composite TFT). Here with the optimized strategy to arrange the incorporated CdS NWs with good alignment, we were able to increase the photoresponsivity to greater than 8.0 A W^{-1} under the same measurement conditions, as shown in Figure 4f. Meanwhile, the mobility of the a-InZnO/(aligned-CdS-NW) composite TFT was further improved to 37.6 cm^2 V^{-1} s^{-1} (based on the transfer characteristics available the SI, Figure S5b). These results indicate that by aligning the NWs in the composite active channel, the performance of these composite TFTs with amorphous metal oxide and crystalline NWs could be much enhanced.

For transparent applications, we fabricated a composite thin film with aligned SnO_2 NWs on 30-nm HfO_2-coated indium tin oxide (ITO) glass, and 50-nm ITO was employed for the source/drain electrodes with the magnetron sputtering method, as shown in **Figure 5**a. Figure 5b is the UV–vis transmittance spectra of the actual device, with an inset optical image indicating the transparency. Typical *I–V* characteristics of a-IGZO/(aligned-SnO_2-NW) composite TFTs are shown in Figure 5c and d. We extracted the field-effect mobility (μ) from the I_{ds}–V_g curve in Figure 5c, leading to a reasonable result of 94.8 cm^2 V^{-1} s^{-1},

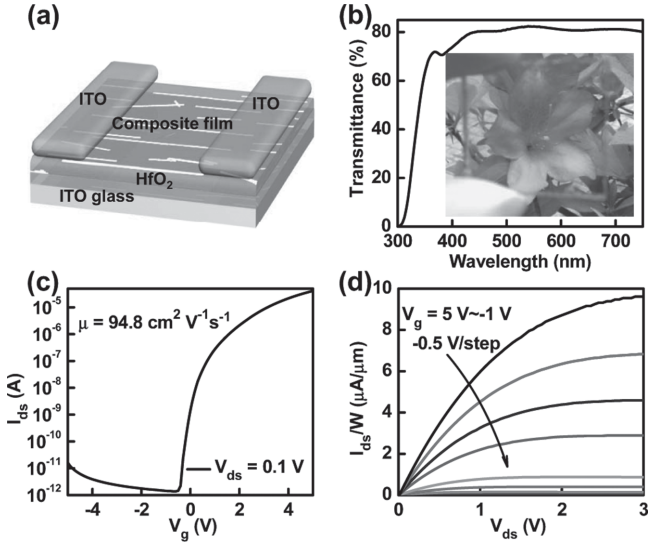

Figure 5. Performance of the transparent a-IGZO/(aligned-SnO_2-NW) composite TFTs on ITO. a) Schematic of the transparent device. b) The UV–vis transmission spectra of the real device; inset: an optical image confirming the transparency. c) Typical transfer characteristics of the transparent a-IGZO/(aligned-SnO_2-NW) composite TFTs. d) The output characteristics of the device showing the reasonable current density.

which is comparable to that of the TFTs fabricated on silicon oxide. And the subthreshold slope was also improved from 770 mV per decade on a SiO_2/Si substrate to be 120 mV per decade on the HfO_2/ITO glass, which was caused by the larger capacitance of the HfO_2 layer and the optimized interface between the HfO_2 and composite thin film. These results indicate that a-IGZO/(SnO_2-NW) composite thin films are stable and could be generalized to other substrates for transparent applications.

In summary, the carrier mobility of the a-IGZO thin films was improved by incorporating the SnO_2 NWs. Moreover, by aligning the incorporated SnO_2 NWs, the mobility of the a-IGZO/(aligned-SnO_2-NW) composite TFT was promoted to 109.0 cm^2 V^{-1} s^{-1} with an on-current density of 61.4 μA $μm^{-1}$ for a 10-μm channel length. This result has surpassed that of single-crystalline InGaZnO and is comparable with that of polysilicon. Last but not least, we demonstrated transparent TFTs by fabricating the a-IGZO/(aligned-SnO_2-NW) composite thin films on HfO_2-coated ITO glass substrates, which suggests that our approach is highly versatile and can be applied to other substrates for transparent electronics.

Experimental Section

Preparation of NWs: The SnO_2 NWs used in this work were synthesized with a chemical vapor deposition method based on the vapor–liquid–solid mechanism. NW growth was carried out in a single-zone horizontal tube furnace with SnO_2/C (weight ratio of 10:1) as the source, and Si coated with 1-nm Au served as the growth substrate. After 20 min of purging, the furnace was heated up to 1050 °C for 30 min with an O_2/Ar mixed gas (volume ratio of 1:99) and rate of 200 sccm. The furnace was then cooled down to room temperature naturally. Finally, SnO_2 NWs were obtained on the substrate with uniform composition across the entire substrate, and the NWs were of good uniformity, with tens of micrometers in length, and 80–100 nm in diameter.

Precursor Preparation: Metal precursors were dissolved in ethanolamine/2-methoxyethanol with a volume ratio of 0.92:100. The molar ratio of In:Ga:Zn was set to 1:1:1, while the total concentration of metal ions was maintained at 0.05 M. After 2 h of vigorous stirring, a stable transparent solution was formed for each precursor solution. Finally, the as-prepared NWs with specific weight concentrations were dispersed in solutions by an ultrasonic process for 5 min in order to fabricate the a-IGZO/(random-SnO_2-NW) composite TFTs. For the a-IGZO/(aligned-SnO_2-NW) composite TFTs, the contact-printing method was used to arrange the SnO_2 NWs in good alignment.

Thin-Film Deposition: 100-nm SiO_2/p^+-Si wafers and ITO glass with 30-nm HfO_2 layers were used as the starting substrates. The cut pieces were thoroughly washed with copious amounts of anhydrous ethanol and dried with an N_2 blower. The clean substrates were further treated with oxygen plasma for 5 min. The a-IGZO/(SnO_2-NW) thin films were formed using the spin-coating method at a speed of 3000 rpm for 60 s. The films were then prebaked on a hotplate at 150 °C for 10 min to remove the organic solvent. This process was repeated 3 times to achieved the desired thickness. Finally, the as-prepared thin films were annealed on the hotplate at 400 °C for 40 min under ambient conditions.

TFT Fabrication and Microscopic Characterization: Two-step photolithography was employed to fabricate the TFTs. First, photolithography and a wet etch (dipped into 10% HCl etchant for 2 min) were carried out to divide the as-prepared thin film into isolated pads, which could suppress the gate leakage current. The second step of photolithography was conducted to define the source and drain electrodes (S/D). The Cr/Au (15 nm/40 nm) electrodes were deposited by thermal evaporation for the electrical measurements on the SiO_2/Si substrates. To fabricate the transparent TFTs array on glass, 50-nm-thick

ITO was deposited by magnetron sputtering, which was also employed for the transparent source/drain electrodes. Electron beam lithography (JEOL 6510 with NPGS) was employed to fabricate a single-NW device. The optical images were captured by an Olympus BX51M microscope.

Electrical Measurements: Electrical measurements were performed with the Lake Shore TTPX Probe Station and Agilent 4155C Semiconductor Parameter Analyzer. For the transport characteristics in the dark, p^+-Si served as the back-gate electrodes, and the gate bias was swept from –50 to +50 V. For all of the photoresponse tests, the channel was first depleted by a default gate bias (the value of the on-current voltage, V_{on}, in the dark) on the back-gate electrode. A mechanical chopper in front of the laser source (CEL-HXF300) was driven by an adjustable power supply. Finally, a source–drain voltage of 0.1 V was set to read out the signal.

Supporting Information

Supporting Information is available from the Wiley Online Library or from the author.

Acknowledgements

We acknowledge the 973 grant of MOST (Nos. 2011CB932700 and 2013CBA01604), MOE (20120141110054), the NSFC grants (Nos. 11104207, 61222402, 11322441, 11274331 and 61376085), Hubei Provincial Natural Science Foundation (2012FFA042), the grant (SYSJJ2013–05) of the State Key Laboratory of Silicate Materials for Architectures at Wuhan University of Technology, the Natural Science of Jiangsu Grant (BK2011348), X.L. and Z.F. acknowledge partial financial support from Special Research Fund Initiative (SRFI11EG17-B and SRF11EG17PG-B) from HKUST. as well as GRF 623112 from the Hong Kong Research Grant Council. The authors acknowledge James Torley for critical reading of the manuscript.

Received: April 16, 2014
Revised: July 22, 2014
Published online:

[1] T. Alford, P. Shetty, N. Theodore, N. Tile, D. Adams, J. Mayer, *Thin Solid Films* **2008**, *516*, 3940.
[2] J.-S. Yoo, S.-H. Jung, Y.-C. Kim, S.-C. Byun, J.-M. Kim, N.-B. Choi, S.-Y. Yoon, C.-D. Kim, Y.-K. Hwang, I.-J. Chung, *J. Disp. Technol.* **2010**, *6*, 565.
[3] H. Yabuta, M. Sano, K. Abe, T. Aiba, T. Den, H. Kumomi, K. Nomura, T. Kamiya, H. Hosono, *Appl. Phys. Lett.* **2006**, *89*, 112123.
[4] P. Carcia, R. McLean, M. Reilly, *Appl. Phys. Lett.* **2006**, *88*, 123509.
[5] L. Han, K. Song, P. Mandlik, S. Wagner, *Appl. Phys. Lett.* **2010**, *96*, 042111.
[6] A. Nathan, A. Kumar, K. Sakariya, P. Servati, S. Sambandan, D. Striakhilev, *IEEE J. Solid-State Circuits* **2004**, *39*, 1477.
[7] J. S. Park, W.-J. Maeng, H.-S. Kim, J.-S. Park, *Thin Solid Films* **2012**, *520*, 1679.
[8] K. Banger, Y. Yamashita, K. Mori, R. Peterson, T. Leedham, J. Rickard, H. Sirringhaus, *Nat. Mater.* **2010**, *10*, 45.
[9] W. Lim, E. Douglas, S.-H. Kim, D. Norton, S. Pearton, F. Ren, H. Shen, W. Chang, *Appl. Phys. Lett.* **2009**, *94*, 072103.
[10] E. M. Fortunato, P. M. Barquinha, A. Pimentel, A. M. Gonçalves, A. J. Marques, L. M. Pereira, R. F. Martins, *Adv. Mater.* **2005**, *17*, 590.
[11] X. Liu, C. Wang, X. Xiao, J. Wang, S. Guo, C. Jiang, W. Yu, W. Hu, J. Li, L. Liao, *Appl. Phys. Lett.* **2013**, *103*, 223108.
[12] X. Liu, C. Wang, B. Cai, X. Xiao, S. Guo, Z. Fan, J. Li, X. Duan, L. Liao, *Nano Lett.* **2012**, *12*, 3596.
[13] T. Takahashi, K. Takei, E. Adabi, Z. Fan, A. M. Niknejad, A. Javey, *ACS Nano* **2010**, *4*, 5855.
[14] X. Duan, C. Niu, V. Sahi, J. Chen, J. W. Parce, S. Empedocles, J. L. Goldman, *Nature* **2003**, *425*, 274.
[15] E. N. Dattoli, Q. Wan, W. Guo, Y. Chen, X. Pan, W. Lu, *Nano Lett* **2007**, *7*, 2463.
[16] G. Shen, J. Xu, X. Wang, H. Huang, D. Chen, *Adv. Mater.* **2011**, *23*, 771.
[17] K. Nomura, H. Ohta, K. Ueda, T. Kamiya, M. Hirano, H. Hosono, *Science* **2003**, *300*, 1269.
[18] Z. Meng, M. Wang, M. Wong, *IEEE Trans. Electron Devices* **2000**, *47*, 404.
[19] T.-M. Pan, C.-J. Chang, *Semicond. Sci. Technol.* **2011**, *26*, 075004.
[20] J. C. Park, H.-N. Lee, S. Im, *ACS Appl. Mater. Interfaces* **2013**, *5*, 6990.
[21] X. Zou, X. Liu, C. Wang, Y. Jiang, Y. Wang, X. Xiao, J. C. Ho, J. Li, C. Jiang, Q. Xiong, *ACS Nano* **2012**, *7*, 804.
[22] Z. Fan, J. C. Ho, Z. A. Jacobson, R. Yerushalmi, R. L. Alley, H. Razavi, A. Javey, *Nano Lett.* **2008**, *8*, 20.
[23] X. Liu, Y.-Z. Long, L. Liao, X. Duan, Z. Fan, *ACS Nano* **2012**, *6*, 1888.
[24] Z. Fan, J. C. Ho, Z. A. Jacobson, H. Razavi, A. Javey, *Proc. Natl. Acad. Sci. USA* **2008**, *105*, 11066.
[25] M. Kim, J. H. Jeong, H. J. Lee, T. K. Ahn, H. S. Shin, J.-S. Park, J. K. Jeong, Y.-G. Mo, H. D. Kim, *Appl. Phys. Lett.* **2007**, *90*, 212114.
[26] R. Chen, W. Zhou, M. Zhang, M. Wong, H. S. Kwok, *Thin Solid Films* **2013**, *548*, 572.
[27] M. J. Kim, D.-K. Choi, *Microelectron. Reliab.* **2012**, *52*, 1346.
[28] G.-W. Hsieh, F. M. Li, P. Beecher, A. Nathan, Y. Wu, B. S. Ong, W. I. Milne, *J. Appl. Phys.* **2009**, *106*, 123706.
[29] C. Wang, X. Liu, X. Xiao, Y. Liu, W. Chen, J. Li, G. Shen, L. Liao, *IEEE Electron Device Lett.* **2013**, *34*, 0741.
[30] J. Yao, L. Gong, L. Xie, S. Zhang, *Thin Solid Films* **2013**, *527*, 21.
[31] J. Wang, K. Li, X. Zhong, Y. Zhou, X. Fang, C. Tang, Y. Bando, *Nanoscale Res. Lett.* **2009**, *4*, 1135.
[32] G. Konstantatos, M. Badioli, L. Gaudreau, J. Osmond, M. Bernechea, F. P. G. de Arquer, F. Gatti, F. H. Koppens, *Nat. Nanotechnol.* **2012**, *7*, 363–368.
[33] Z. Zhang, C. Jin, X. Liang, Q. Chen, L.-M. Peng, *Appl. Phys. Lett.* **2006**, *88*, 073102.
[34] H. M. Manohara, E. W. Wong, E. Schlecht, B. D. Hunt, P. H. Siegel, *Nano Lett.* **2005**, *5*, 1469.
[35] X. Liu, X. Yang, M. Liu, Z. Tao, Q. Dai, L. Wei, C. Li, X. Zhang, B. Wang, A. Nathan, *Appl. Phys. Lett.* **2014**, *104*, 113501.
[36] K. Ghaffarzadeh, A. Nathan, J. Robertson, S. Kim, S. Jeon, C. Kim, U. Chung, J.-H. Lee, *Appl. Phys. Lett.* **2010**, *97*, 113504.
[37] W.-T. Chen, H.-W. Zan, *IEEE Electron Device Lett.* **2012**, *33*, 77.
[38] D. Zhang, L. Gan, Y. Cao, Q. Wang, L. Qi, X. Guo, *Adv. Mater* **2012**, *24*, 2715.
[39] M. Kimura, T. Hasegawa, K. Ide, K. Nomura, T. Kamiya, H. Hosono, *IEEE Electron Device Lett.* **2012**, *33*, 384.
[40] J. Suehiro, N. Nakagawa, S.-I. Hidaka, M. Ueda, K. Imasaka, M. Higashihata, T. Okada, M. Hara, *Nanotechnology* **2006**, *17*, 2567.
[41] L. Hu, J. Yan, M. Liao, L. Wu, X. Fang, *Small* **2011**, *7*, 1012.
[42] T. Chang, C. Chiu, S. Chang, T. Tsai, T. Yang, Z. Huang, W. Weng, *Appl. Phys. Lett.* **2013**, *102*, 221104.
[43] T.-Y. Hsieh, T.-C. Chang, T.-C. Chen, Y.-C. Chen, Y.-T. Chen, P.-Y. Liao, A.-K. Chu, W.-W. Tsai, W.-J. Chiang, J.-Y. Yan, *Appl. Phys. Lett.* **2012**, *101*, 212104.
[44] X. Liu, L. Jiang, X. Zou, X. Xiao, S. Guo, C. Jiang, X. Liu, Z. Fan, W. Hu, X. Chen, *Adv. Mater.* **2014**, *26*, 2919.
[45] A. Balducci, M. Marinelli, E. Milani, M. Morgada, A. Tucciarone, G. Verona-Rinati, M. Angelone, M. Pillon, *Appl. Phys. Lett.* **2005**, *86*, 193509.
[46] W. Yang, S. Hullavarad, B. Nagaraj, I. Takeuchi, R. Sharma, T. Venkatesan, R. Vispute, H. Shen, *Appl. Phys. Lett.* **2003**, *82*, 3424.
[47] D. Caputo, G. de Cesare, A. Nascetti, R. Negri, R. Scipinotti, *IEEE Sens. J.* **2007**, *7*, 1274.